

# A magnitude-limited catalogue of unresolved white dwarf-main sequence binaries from *Gaia* DR3

Alberto Rebassa-Mansergas<sup>1,2\*</sup>, Enrique Solano<sup>3</sup>, Alex J. Brown<sup>4</sup>, Steven G. Parsons<sup>5</sup>, Raquel Murillo-Ojeda<sup>3</sup>, Roberto Raddi<sup>1</sup>, Maria Camisassa<sup>1</sup>, Santiago Torres<sup>1,2</sup>, Jan van Roestel<sup>6</sup>

<sup>1</sup> Departament de Física, Universitat Politècnica de Catalunya, c/Esteve Terradas 5, 08860 Castelldefels, Spain

<sup>2</sup> Institut d'Estudis Espacials de Catalunya (IEEC), C/Esteve Terradas, 1, Edifici RDIT, 08860 Castelldefels, Spain

<sup>3</sup> Centro de Astrobiología (CAB), CSIC-INTA, Camino Bajo del Castillo s/n, 28692 Villanueva de la Cañada, Madrid, Spain

<sup>4</sup> Hamburger Sternwarte, University of Hamburg, Gojenbergsweg 112, 21029 Hamburg, Germany

<sup>5</sup> Astrophysics Research Cluster, School of Mathematical and Physical Sciences, University of Sheffield, Sheffield S3 7RH, UK

<sup>6</sup> Anton Pannekoek Institute for Astronomy, University of Amsterdam, 1090 GE, Amsterdam, The Netherlands

Received ; accepted

## ABSTRACT

**Context.** Binary stars containing a white dwarf and a main-sequence star, WDMS binaries, can be used to study a wide range of aspects of stellar astrophysics.

**Aims.** We build a magnitude-limited sample of unresolved WDMS binaries from *Gaia* DR3 to enlarge these studies.

**Methods.** We look for WDMS with available spectra whose location in the *Gaia* colour-magnitude diagram bridges between the evolutionary sequences of single white dwarfs and the main-sequence. To exclude spurious sources we apply quality cuts on the *Gaia* photometry and astrometry and we fit the SED (spectral energy distribution) of the objects with VOSA (Virtual Observatory SED Analyser) to exclude single sources. We further clean the sample via visual inspection of the *Gaia* spectra and publicly available images of the objects. We re-fit the SEDs of the finally selected WDMS with VOSA using composite models to measure their stellar parameters and we search for eclipsing systems by inspecting available ZTF and CRTS light curves.

**Results.** The catalogue consists of 1312 WDMS and we manage to derive stellar parameters for 435. This is because most WDMS are dominated by the main-sequence companions, making it hard to derive parameters for the white dwarfs. We also identify 67 eclipsing systems and estimate a lower limit to the completeness of the sample to be  $\approx 50\%$  ( $\approx 5\%$  if we consider that not all WDMS in the studied region have *Gaia* spectra).

**Conclusions.** Our catalogue increases by one order of magnitude the volume-limited sample we presented in our previous work. Despite the fact that the sample is incomplete and suffers from heavy observational biases, it is well characterised and can therefore be used to further constrain binary evolution by comparing the observed properties to those from synthetic samples obtained modeling the WDMS population in the Galaxy, taking into account all selection effects.

**Key words.** (Stars:) white dwarfs; (Stars:) binaries (including multiple): close

## 1. Introduction

White dwarf-main sequence (WDMS) binaries are binary stars formed by a white dwarf, the most common stellar remnant, and a main-sequence star. They descend from main-sequence binaries in which the primary, more massive star, had time to evolve out of the main-sequence. Two general pathways lead to the formation of a WDMS.

The first one involves mass transfer interactions that usually take place once the primary becomes a red giant, or an asymptotic giant star. That is, the initial main-sequence binary orbital separation is short enough ( $\lesssim 10$  AU; Farihi et al. 2010) for the giant star to overfill its Roche-lobe and to transfer mass to the secondary, less massive, companion. Given that the mass transfer is generally dynamically unstable, the system is thought to evolve through a common envelope phase (Paczynski 1976; Webbink 2008) in which the core of the giant and the secondary star are surrounded by common material formed by the outer layers of the giant – that have been transferred to but not accreted by the companion – and friction considerably reduces

the orbital separation, hence orbital period to a few hours/days (Rebassa-Mansergas et al. 2008; Nebot Gómez-Morán et al. 2011). WDMS with orbital periods as large as  $\approx 1000$  days are also suggested to be the outcome of common envelope evolution (Yamaguchi et al. 2024), being stable non-conservative mass transfer the alternative evolutionary path for such long-period systems (Hallakoun et al. 2024; Garbutt et al. 2024). It is expected that these post-common envelope binaries account for approximately 25% of the initial main-sequence binaries (Willems & Kolb 2004).

The second scenario, encompassing the remaining  $\approx 75\%$  of the cases, does not involve mass transfer episodes, since the initial main sequence binary orbits are wide enough to avoid them, and consequently the primary star evolves like a single star. In these cases, the orbital periods of the WDMS binaries are of the order of hundreds to thousands of days.

Both wide WDMS binaries that evolved like isolated stars and post-common envelope binaries have been of extreme value to tackle a wide diversity of issues. For instance, since the white dwarfs in wide WDMS binaries can be used to measure stellar ages, studies of such systems have constrained the age-

\* E-mail: alberto.rebassa@upc.edu

metallicity relation (Rebassa-Mansergas et al. 2016a, 2021a) and the age-velocity dispersion relation (Raddi et al. 2022) in the solar neighbourhood, as well as the age-activity-rotation relation of low-mass main-sequence stars (Rebassa-Mansergas et al. 2013, 2023; Chiti et al. 2024). They can also be used to test the white dwarf mass-radius relation (Arseneau et al. 2024; Raddi et al. 2025) and the initial-to-final mass relation (Zhao et al. 2012; Barrientos & Chanamé 2021). On the other hand, close post-common envelope binaries allow constraining the efficiency of common envelope ejection (Zorotovic et al. 2010; Camacho et al. 2014; Cojocaru et al. 2017; Grondin et al. 2024), the mass-radius relation of white dwarfs (Parsons et al. 2017), low-mass main-sequence stars (Parsons et al. 2018) and even brown dwarfs (Parsons et al. 2025) and sub-dwarf stars (Rebassa-Mansergas et al. 2019) via the analysis of eclipsing systems, the origin of low-mass white dwarfs (Rebassa-Mansergas et al. 2011), angular momentum losses due to magnetic braking (Schreiber et al. 2010; Zorotovic et al. 2016) and the origin of magnetism in white dwarfs (Marsh et al. 2016; Schreiber et al. 2021).

The first large catalogue of  $\approx 3200$  WDMS binaries was built thanks to the mining of the Sloan Digital Sky Survey (SDSS; Eisenstein et al. 2011) spectroscopic database (Rebassa-Mansergas et al. 2012, 2016b), closely followed by the spectroscopic catalogue of  $\approx 900$  additional systems (Ren et al. 2018) from the Large Sky Area Multi-Object Fiber Spectroscopic Telescope (LAMOST; Cui et al. 2012). Since these samples are largely affected by selection effects, in particular by the fact that earlier type than M companions outshine the white dwarfs in the optical (Rebassa-Mansergas et al. 2010), efforts have been placed to combine ultraviolet photometry with optical photometry and/or spectroscopy that allowed the identification of thousands of WDMS binaries containing F, G and K companions (Parsons et al. 2016; Rebassa-Mansergas et al. 2017; Ren et al. 2020; Anguiano et al. 2022; Nayak et al. 2024; Sidharth et al. 2024).

A potential issue from the above studies is that they are all magnitude-limited, which makes it difficult to unveil the underlying population unless population synthesis studies are taken into account (Davis et al. 2010; Toonen & Nelemans 2013; Torres et al. 2022). In this sense, the astrometry and photometry provided by the *Gaia* satellite (Gaia Collaboration et al. 2018, 2023) allowed mitigating this effect, as it became possible to build the first volume-limited sample of 112 well-characterised candidates within 100 pc from the early data release 3 (Rebassa-Mansergas et al. 2021b). In this analysis, we defined a region in the *Gaia*  $G_{\text{abs}}$  vs.  $G_{\text{BP}} - G_{\text{RP}}$  diagram to exclude single white dwarfs and main-sequence stars and derived white dwarf and main-sequence stellar parameter distributions that clearly differed from those obtained from magnitude-limited samples. Moreover, a direct comparison with the parameter distributions obtained from numerical simulations that reproduced the *Gaia* population in the Galaxy provided additional valuable insight into binary star formation and evolution (Santos-García et al. 2025). Unfortunately, despite being a volume-limited sample, the *Gaia* catalogue was revealed to be highly incomplete, as most of the WDMS binaries are expected to have *Gaia* colours very similar to those of main-sequence stars (Santos-García et al. 2025), which were excluded from the analysis. As mentioned above, these systems are difficult to identify since the main-sequence companions outshine the white dwarfs in the optical. A promising way to move forward is to make use of artificial intelligence algorithms to differentiate between single main-sequence stars and WDMS binaries via the analysis of available *Gaia* spectra from its data release 3 (Echeverry et al. 2022; Li et al. 2025; Pérez-Couto et al. 2025).

In this work, our motivation is to build up the *Gaia* WDMS binary sample we presented in Rebassa-Mansergas et al. (2021b) by not implementing any distance cut, but maintaining the focus in the bridge region of the *Gaia* colour-magnitude diagram between single white dwarfs and single main-sequence stars. That is, we aim at providing a magnitude-limited but well-characterised sample from *Gaia* that can be directly compared to the output of numerical simulations such as those we implemented in Santos-García et al. (2025). This will allow deriving further constraints on binary evolution theory.

In Section 2 we introduce the WDMS binary sample and in Section 3 we attempt to derive their stellar parameters. In Section 4 we compare our sample to other works in the literature. In Section 5 we identify eclipsing WDMS among our objects and conclude the work in Section 6.

## 2. The WDMS sample

We follow basically the same criteria as Rebassa-Mansergas et al. (2021b) to build the WDMS binary sample from *Gaia* data release (DR) 3 (Gaia Collaboration et al. 2023). That is, we consider all objects in the intermediate region between single white dwarfs and single main-sequence stars in the *Gaia* colour-magnitude diagram with parallax over error and  $G$ ,  $G_{\text{BP}}$ ,  $G_{\text{RP}}$  flux over error parameters greater than 10. However, in this work we do not impose any distance limit and we focus the search to objects with available *Gaia* spectra. As we will see later, this condition (having available *Gaia* spectra) affects the completeness of our catalogue. However, it is required since we intend to measure the stellar parameters of the identified candidates from these spectra. Moreover, visual inspection greatly helps in confirming the binary nature of the candidates by identification of the two components in the available spectra. This resulted in 126 787 selected sources, illustrated in the top left panel of Figure 1.

To reduce contaminants, defined as sources that are not WDMS, from our selected candidates, we first applied a condition on the excess factor parameter provided by *Gaia*. This parameter is defined as  $C = (F_{\text{BP}} + F_{\text{RP}})/F_G$  (Evans et al. 2018), where  $F$  denotes flux in the *Gaia* bands, and it should be close to 1. Thus, any object with deviations from  $C = 1$  may be associated to internal calibration issues. It has to be emphasised that one of the possible causes for having a large excess factor is binarity, that is *Gaia* sees two sources that form a partially resolved system. As noted by Riello et al. (2021),  $C$  is colour dependent and so they defined  $C^* = C - f(G_{\text{BP}}, G_{\text{RP}})$ , where the function  $f$  provides the expected excess at a given colour. In other words, by correcting the expected excess, any object with a  $|C^*|$  value larger than zero can be considered as a potential source affected by calibration issues. It depends on the user to be as restrictive as necessary to exclude such sources. To that end we followed the same approach as Rebassa-Mansergas et al. (2021b) and removed all sources with:

$$|C^*| \geq 0.3, \quad G_{\text{BP}} - G_{\text{RP}} < 0.5; \quad (1)$$

$$|C^*| \geq 0.2, \quad 0.5 \leq G_{\text{BP}} - G_{\text{RP}} \leq 4; \quad (2)$$

$$|C^*| \geq 0.1, \quad G_{\text{BP}} - G_{\text{RP}} > 4. \quad (3)$$

This cut reduced the WDMS candidates to 82 021. It should be noted that these cuts are different from the traditional criteria suggested by Riello et al. (2021), which is based not only on the  $|C^*|$  value but also on its deviation  $\sigma$ . Thus, the user may exclude objects by simply applying a  $|C^*| > N\sigma$  cut by fixing a value of

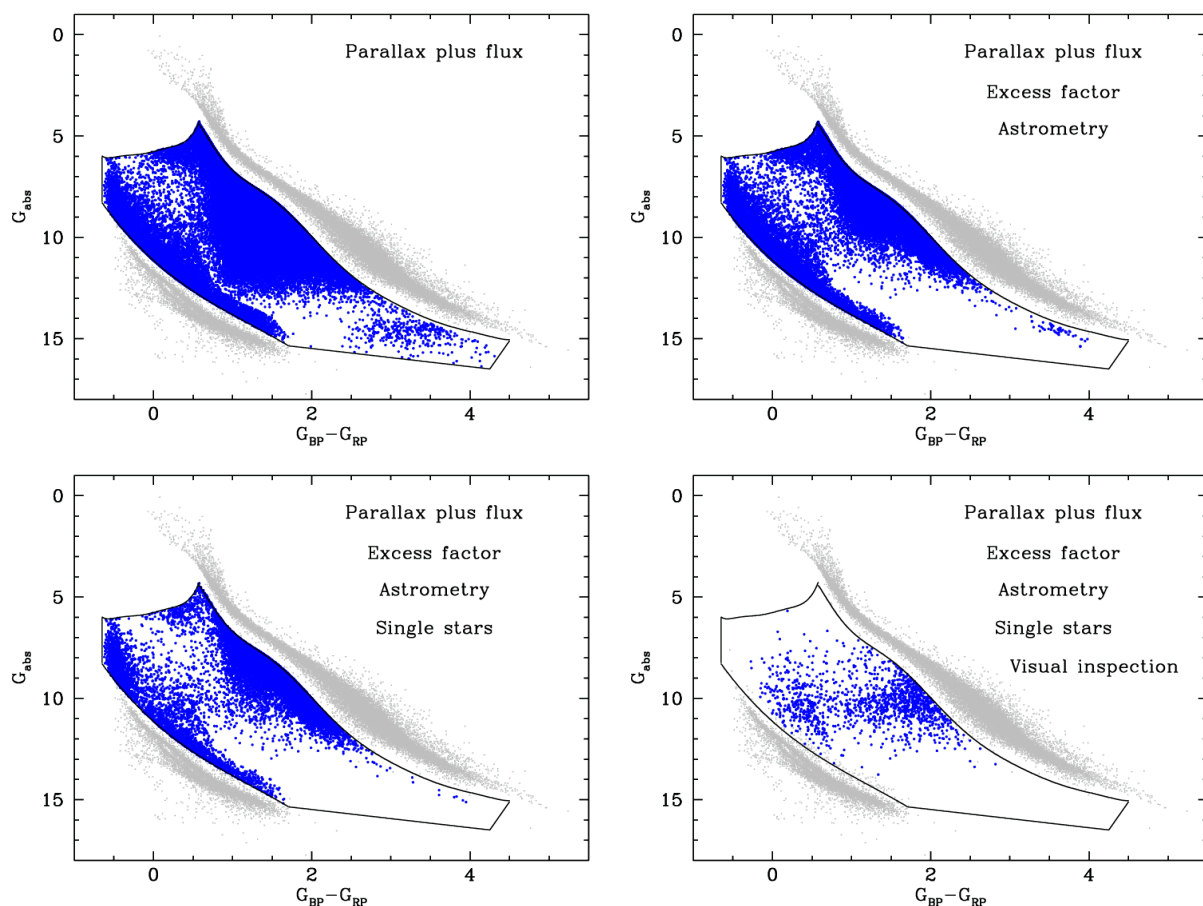


**Fig. 1.** Results of our criteria imposed on the *Gaia* data release 3 data base to select WDMS binaries (see details in Section 2). Top left: in blue the 126 787 sources within the WDMS binary region defined by the black solid lines (Rebassa-Mansergas et al. 2021b) with available spectra and satisfying parallax and flux relative errors above 10%. The gray dots illustrate the expected location of single white dwarfs and main-sequence stars. Top right: the same after applying our excess factor and astrometry (RUWE, `astrometric_excess_noise` and `astrometric_excess_noise_sig`) cuts, which leaves 62 386 objects. Bottom left: the same after excluding single stars using VOSA, leaving 13 905 candidates. Bottom right: the final catalogue of 1312 WDMS binaries after visual inspection of the *Gaia* spectra.

$N$ . However, even when using  $N = 5$ , which is expected to be a largely conservative cut (meaning that most of the excluded sources should indeed be associated to spurious data), we ended up excluding clear WDMS binaries from the sample. In fact, any cut in the excess noise will unavoidably exclude real WDMS, thus affecting the completeness of the final sample. This issue will be later discussed in Section 4.

So far, we have only applied one constraint to the *Gaia* astrometry, excluding objects with parallax relative errors larger than 10%. Thus, an additional way to further exclude contaminants from our list is by removing objects associated with bad astrometric solutions. In particular, *Gaia* provides three parameters that can be used for such purpose (Lindgren et al. 2012): the renormalised unit weight error RUWE, which should be near 1.0 for point sources that are well fitted by a single-star model to their astrometric observations; the `astrometric_excess_noise` parameter, which quantifies the agreement between the observations of a given object and the best-fit astrometric model; and the `astrometric_excess_noise_sig` parameter, which gives the significance of the `astrometric_excess_noise`. It is suggested by *Gaia* that objects with  $\text{RUWE} > 1.4$ ,  $\text{astrometric\_excess\_noise} > 2$  or  $\text{astrometric\_excess\_noise\_sig} > 2$  may have issues with their astrometric solutions. Since larger than canonical values of RUWE are also possible due to binarity, we adopted all sources from our list with RUWE values smaller than 3, instead of 1.4. This is jus-

tified by looking at figure 4 (top left panel) of Belokurov et al. (2020), where less than 5% of the 801 spectroscopic binaries considered have RUWE values larger than 3. In the same way, to avoid missing possible binaries, we excluded objects satisfying  $\text{astrometric\_excess\_noise} > 3$  &  $\text{astrometric\_excess\_noise\_sig} > 3$ , rather than the canonical value of 2. As a consequence, the number of WDMS binaries in our list was further reduced to 62 386 (see the top right panel of Figure 1). In more than 99% of the cases, the sources were excluded due to the RUWE condition, whilst the rest of objects had a RUWE value smaller than 3 but large values of both `astrometric_excess_noise` and `astrometric_excess_noise_sig`. This means that our cuts in these last two parameters are basically irrelevant. In Section 4 we will discuss the impact of the adopted RUWE cut in the completeness of our catalogue.

It is worth noting that there are more *Gaia* parameters that the user can potentially explore to exclude possible contaminants, such as `astrometric_sigma5d_max`<sup>1</sup> (see, for example Gentile Fusillo et al. 2019), the astrometric fidelity parameter able to classify spurious data (Rybizki et al. 2022), or even al-

<sup>1</sup> A five-dimensional equivalent to the semi-major axis of the *Gaia* position error ellipse. Useful for filtering out cases where one of the five parameters, or some linear combination of several parameters, is bad.



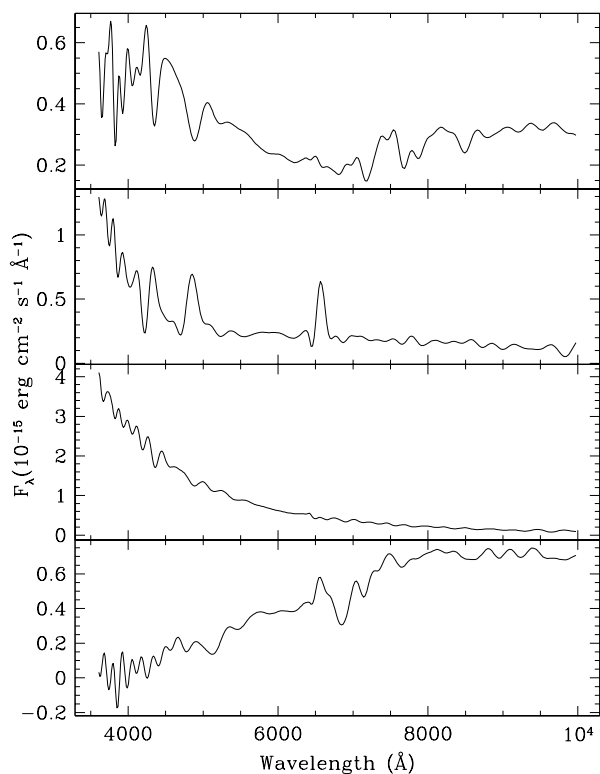


**Fig. 2.** Example spectra of a WDMS binary (top, *Gaia* ID 1057463111970047488; note that in this work we use the DR3 IDs), a cataclysmic variable (middle top, *Gaia* ID 3703726255561754880), a hot white dwarf (middle bottom, *Gaia* ID 1060659289192635904) and a low-mass low-metallicity subdwarf as revealed by the broad absorption feature at  $\sim 7000$  Å (bottom, *Gaia* ID 1048217078174314496) arising from the visual inspection of the *Gaia* spectra.

ternative quantities such as the local unit weight error defined by [Penoyre et al. \(2022\)](#). However, we do not implement further quality cuts in astrometry and proceed in reducing the number of contaminants (in particular single sources expected near the locus of single white dwarfs and main-sequence stars) as follows.

We used *Gaia*XPy to convert the *Gaia* spectra of each source into synthetic J-PAS (Javalambre Physics of the Accelerating Universe Astrophysical Survey; [Marín-Franch et al. 2012](#); [Benítez et al. 2014](#)) photometry, which consists of 57 filters continuously sampling the spectrum between 3700 and 9200 Å, thus obtaining their spectral energy distributions (SEDs). We then fitted the resulting SEDs using the Virtual Observatory SED Analyser (VOSA; [Bayo et al. 2008](#))<sup>2</sup> tool. In the fitting process we only took into account those points in the SED with relative flux errors less than 10%, and all data above 4000 Å, since the signal-to-noise ratio under this value is generally substantial. This implied 1004 objects were excluded simply because they did not have enough reliable points in their SEDs. Moreover, we adopted the geometric distances for each source from [Bailer-Jones \(2023\)](#), the extinction from the 3D maps of [Lallement et al. \(2014\)](#) and we did not use upper limits in the fits. In a first step, we used the CIFIST ([Allard et al. 2013](#)) grid (effective temperatures between 2200 and 7000 K, surface gravities between 4.5 and 5.5 dex, typical values for main-sequence stars, and solar metallicity) to exclude 37 712 objects with  $\chi^2$  fit values less than 10. In 99.5% of these cases, the corresponding visual goodness of

fit  $V_{\text{gfb}}$ <sup>3</sup> was less than 2, with a maximum value of 7.2. Since  $V_{\text{gfb}}$  values of less than 15 are usually taken as a validation for a good fit, these excluded objects should indeed be very likely single main sequence-stars, possibly affected by extinction. It is worth noting that we initially applied a  $V_{\text{gfb}} < 15$  cut to filter out single main-sequence star candidates; however this resulted in a non-negligible fraction of excluded WDMS binaries and, as a consequence, we opted for the approach described above. In a second step, we fitted the remaining 24 674 sources with the [Koester \(2010\)](#) model grid of hydrogen-rich white dwarfs (effective temperatures between 5000 and 40 000 K and surface gravities between 6.5 and 9.5 dex). We excluded 10 769 sources, very likely single or double<sup>4</sup> white dwarfs, with  $\chi^2$  fit values less than 10, which correspond to  $V_{\text{gfb}}$  values of less than 3 in 98% of the cases, with a maximum value of 8.7. After this exercise, we were left then with 13 905 WDMS binary candidates in our list (see bottom left panel of Figure 1).

We proceeded to visually inspect the *Gaia* spectra of the 13 905 candidates, which resulted in the identification of 1312 genuine WDMS binaries, 155 cataclysmic variables (we identify as such those objects with spectra displaying prominent and broad Balmer emission lines arising from the accretion disk) and 12 438 other sources. Most of these other sources were single hot white dwarfs and low-mass low-metallicity sub-dwarfs according to their *Gaia* spectra. Given that the white dwarf [Koester \(2010\)](#) grid and the [Allard et al. \(2013\)](#) CIFIST grid in VOSA do not include white dwarf model spectra hotter than 40 000 K and low metallicities stars (only solar abundances), respectively, it is not surprising that these objects were not previously considered as single stars, and were therefore not excluded. It is also worth noting that the visual classification of WDMS relies on the identification of both stars in the spectra, which is challenging if one of the components dominates the SED. This is worsened due to the low resolution of the *Gaia* spectra. As a consequence, this process is biased against the identification of WDMS with mild blue/red excess in their spectra. In Section 4 we will evaluate how these issues affect the completeness of our sample. Example spectra of a WDMS binary, a cataclysmic variable, a single hot white dwarf and a single low-metallicity subdwarf star can be seen in Figure 2. We note that the above identified CVs are not included in our WDMS catalogue, since we are focusing on non-accreting binaries. However, it is of course plausible that some WDMS in our sample are detached CVs crossing the period gap.

To finalise, we visually inspected the Pan-STARRS g-band and POSS/DSS blue and red images of our objects by eye and flagged 72 objects that are possibly contaminated by the presence of bright nearby stars. That is, these are candidates for not being real WDMS binaries but contaminated stars by the flux of nearby sources. Two examples are shown in Figure 3.

A summary of the different cuts we have applied, including the fraction of excluded objects, is provided in Table 1. An excerpt of the full 1312 WDMS binary catalogue is included in Table 2. The full table is available at the CDS.

### 3. Stellar parameters

In this section we attempt to derive the stellar parameters of the 1312 WDMS binary candidates. To that end we first use the two-

<sup>3</sup> See details at <http://svo2.cab.inta-csic.es/theory/vosa/helpw4.php?otype=star&action=help&what=fit>

<sup>4</sup> Double white dwarfs are generally located above the single white dwarf locus in the *Gaia* colour-magnitude diagram, well within our area of study. Since their SEDs are virtually identical to those of single white dwarfs, double white dwarfs are also excluded in this exercise.

<sup>2</sup> <http://svo2.cab.inta-csic.es/theory/vosa>

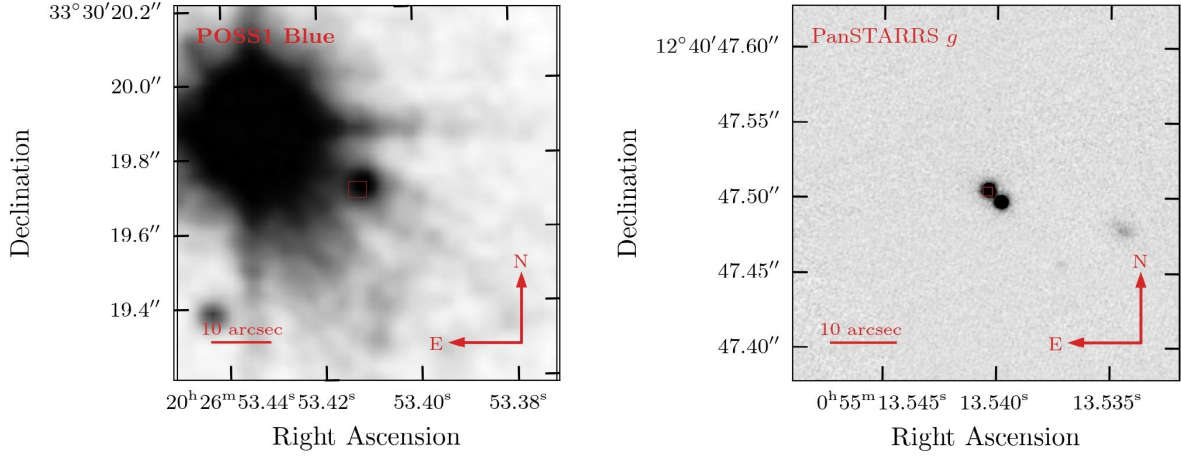


**Fig. 3.** Example images illustrating WDMS candidates (red squares) for being contaminated by the presence of nearby sources. Left panel: POSS/DSS blue image of *Gaia* ID 2055951194776633600. Right panel: Pan-STARRS g-band image of *Gaia* ID 2776554794743195648.

**Table 1.** WDMS selection process from our initial sample to the final catalogue.

Sample	#objects	$f_{\text{abs}}$	$f_{\text{rel}}$
Initial	126 787	-	-
Excess factor cut	82 021	0.65	0.65
Astrometry cuts	62 386	0.49	0.76
Excluding single stars	13 905	0.11	0.22
Visual inspection and final catalogue	1312	0.01	0.09

**Notes.** The initial sample corresponds to those objects within the defined WDMS region with *Gaia* spectra and with parallax and flux over errors greater than 10%.  $f_{\text{abs}}$  and  $f_{\text{rel}}$  give the absolute and relative fractions, respectively

body fit implemented in VOSA. In this case, we complemented the *Gaia* J-PAS synthetic photometry with Galaxy Evolution Explorer (GALEX; Bianchi et al. 2017), Two Micron All Sky Survey (2MASS; Skrutskie et al. 2006) and ALLWISE (Wide-field Infrared Survey Explorer; Wright et al. 2018) photometry associated with good quality flags, and avoiding upper limits in the fit. In the matching process we took into account the *Gaia* proper motions of the targets to compute the position in the epoch 2000 and applied a search radius of 5 arcsec.

We used the low-mass star CIFIST and the hydrogen-rich white dwarf models in the fit, which provided the bolometric luminosities ( $L_{\text{bol}} = 4\pi D^2 F_{\text{bol}}$ , where  $D$  is the distance to each target and  $F_{\text{bol}}$  is the bolometric flux<sup>5</sup>), effective temperatures (from the best-model fit in the grids after re-scaling the flux) and radii (both from the flux scaling factors of both components and the Stefan–Boltzmann equation) for the two components. We subsequently derived the white dwarf surface gravities interpolating the effective temperatures and radii in the hydrogen-rich cooling sequences from La Plata (Althaus et al. 2013; Camisassa et al. 2016, 2019). Finally, we obtained the white dwarf masses from the well-known relation  $g = GM/R^2$ , where  $M$  and  $R$  are the mass and the radius,  $G$  is the gravitational constant and  $g$  is

the surface gravity (note that we obtained  $\log g$  from the cooling sequences).

We visually inspected the two-body fits to evaluate the validity of the results obtained. It became obvious that, in the cases where the secondary star dominates the SED, VOSA was generally unable to find a combination of models that satisfactorily sampled the observed SEDs due to the lack of points available at blue wavelengths. As a consequence, even when the combination of models matched the observed data, we considered most of the results as unreliable since the white dwarfs typically piled up at too low effective temperatures (5000–7000 K) as compared to those from the secondary stars (2800–3000 K). Such low-luminosity white dwarfs would not be visible in the optical against such M star companions. An example is shown in the top panel of Figure 4. To compensate the intrinsically low bolometric fluxes (and luminosities) of the white dwarfs, VOSA tends to yield large radii to those objects, which translates into very low white dwarf masses. This likely explains the excess of extremely low-mass white dwarfs identified in Rebassa-Mansergas et al. (2021b). In Brown et al. (in prep.) we will discuss in detail these issues, but we advance here that all fits resulting in white dwarf effective temperatures of less than 10 000 K should be taken with caution. In other words, the SEDs of WDMS with dominating main-sequence companions have few available points at blue wavelengths in their SEDs, where the white dwarfs are expected to contribute most. As a consequence, the white dwarf parameters tend to be unreliable. Having available GALEX photometry helps to mitigate this effect. However, the visual inspection of the fits also revealed that, in some cases, the best-fit white dwarf model failed at sampling the GALEX photometry (see the middle panel of Figure 4).

Due to the reasons outlined above, we only considered as reliable fits those with white dwarf effective temperatures larger than 10 000 K, white dwarf masses higher than  $0.35 M_{\odot}$  and with the best-fit white dwarf model matching the GALEX data, when available. An example is illustrated in the bottom panel of Figure 4. This resulted in 435 WDMS binaries with reliable fits. The distribution of white dwarf effective temperatures, surface gravities and masses, and secondary star effective temperatures are shown in Figure 5.

Most white dwarfs have effective temperatures between 12 000 and 17 000 K, with a long tail towards higher temperatures, as it is expected from a magnitude-limited sample (see, for example, Rebassa-Mansergas et al. 2010). The white

<sup>5</sup> See <http://svo2.cab.inta-csic.es/theory/vosa/helpw4.php?otype=star&what=intro> for a description on how the bolometric flux is derived.

**Table 2.** An excerpt of the *Gaia* WDMS binary catalogue.

<i>Gaia</i> ID	Ra (deg)	Dec (deg)	par. (mas)	<i>G</i> (mag)	<i>G</i> <sub>BP</sub> (mag)	<i>G</i> <sub>RP</sub> (mag)	<i>T</i> <sub>eff</sub> (WD) (K)	log <i>g</i> (WD) (dex)	<i>M</i> (WD) <i>M</i> <sub>⊙</sub>	<i>T</i> <sub>eff</sub> (MS) (K)	Per. (days)	flag
1006621281985546240	98.37658	61.39074	13.01	14.30	15.08	13.36	14250 ± 125	7.90 ± 0.02	0.55 ± 0.03	3400 ± 50	-	0
1019109878651542272	141.09262	51.04458	7.64	16.05	16.78	15.11	12000 ± 125	7.84 ± 0.03	0.53 ± 0.03	3300 ± 50	-	0
1031612970830684800	123.52560	52.28758	1.94	17.67	17.71	17.42	26000 ± 500	7.38 ± 0.04	0.43 ± 0.04	3100 ± 50	-	0
1031818515080479616	123.54097	53.32249	5.35	16.89	16.97	16.60	17750 ± 125	7.78 ± 0.01	0.52 ± 0.02	2900 ± 50	-	0
1034719400416394752	125.26102	56.39990	6.20	17.34	17.84	16.55	11000 ± 125	7.92 ± 0.03	0.55 ± 0.04	3100 ± 50	-	0
1041938213945851264	128.13788	61.18896	3.62	17.32	17.44	16.97	23000 ± 500	7.87 ± 0.06	0.56 ± 0.07	3100 ± 50	-	0
1057463111970047488	172.28939	66.61785	3.41	17.38	17.71	16.73	- ± -	- ± -	- ± -	- ± -	-	0
1059664849644881152	162.88903	66.56686	4.61	17.11	17.24	16.73	17000 ± 125	7.68 ± 0.02	0.48 ± 0.02	3000 ± 50	-	0
1066494019444338816	150.70489	66.81527	4.43	17.09	17.87	16.09	12750 ± 125	7.82 ± 0.03	0.52 ± 0.03	3200 ± 50	-	0
1068953042840614272	138.95581	67.27441	3.56	16.87	17.52	15.98	18250 ± 125	7.77 ± 0.02	0.52 ± 0.02	3300 ± 50	-	0
1078143894896636672	157.16275	73.18020	11.34	16.91	17.93	15.81	- ± -	- ± -	- ± -	- ± -	-	0
1086336218595221248	113.11450	60.69626	9.44	17.56	18.34	16.59	- ± -	- ± -	- ± -	- ± -	-	0
1089352587012640640	115.49536	64.08135	5.26	15.71	15.81	15.37	20000 ± 312	7.23 ± 0.03	0.36 ± 0.03	3100 ± 50	-	0
1091121396280101504	122.37888	62.95820	3.25	17.02	17.90	16.01	14750 ± 125	7.72 ± 0.02	0.49 ± 0.03	3300 ± 50	-	0
109973634046969472	45.78159	23.29454	4.35	15.35	15.94	14.50	- ± -	- ± -	- ± -	- ± -	-	0
1105873062754421376	99.53318	68.07844	3.45	18.16	18.27	17.82	- ± -	- ± -	- ± -	- ± -	-	1
1106926566694585984	94.80641	69.19361	3.22	16.89	16.83	16.92	23000 ± 500	7.33 ± 0.05	0.40 ± 0.05	2900 ± 50	-	0
1125637127860398848	131.85117	76.31376	8.38	16.61	17.49	15.62	- ± -	- ± -	- ± -	- ± -	-	0
1128036811987813888	155.08710	77.28237	5.40	17.50	18.07	16.67	11500 ± 125	7.97 ± 0.03	0.58 ± 0.04	3100 ± 50	1.38206 <sup>(0)</sup>	0
1132443276634291200	146.52269	80.02909	4.36	17.44	18.15	16.51	12250 ± 125	7.90 ± 0.03	0.55 ± 0.03	3200 ± 50	-	0
...	...	...	...	...	...	...	...	...	...	...	...	...

**Notes.** Included are the *Gaia* source IDs, the coordinates, parallaxes, magnitudes, stellar parameters (note that the effective temperature errors are simply half the step between the available models), orbital periods for the 67 identified eclipsing systems (also including a note indicating if the system is new from this work or has been published before; Section 5) and a flag indicating whether (1) or not (0) the object is possibly contaminated by the presence of nearby bright sources. We provide the stellar parameters only for all WDMS with effective temperatures higher than 10 000 K and masses above 0.35  $M_{\odot}$ . The objects are given in order of ascending source ID. The Per. column is associated to the following references: (0) This work; (1) Brown et al. (2023); (2) Bruch & Diaz (1998); (3) Chen et al. (2020); (4) Kosakowski et al. (2022); (5) Mowlavi et al. (2023); (6) Nebot Gómez-Morán et al. (2009); (7) O’Donoghue et al. (2003); (8) Parsons et al. (2013); (9) Parsons et al. (2015); (10) Priyatikanto et al. (2022); (11) Pyrzas et al. (2009); (12) Pyrzas et al. (2012).

dwarf masses peak at  $\approx 0.5 M_{\odot}$  and the surface gravities at  $\log g \approx 7.8$  dex, in agreement with the volume-limited sample presented in Rebassa-Mansergas et al. (2021b). In that paper we argued these peaks are lower than the canonical values of  $\approx 0.6 M_{\odot}$  and 8 dex presumably due to the fact that unresolved WDMS binaries within 100 pc are likely post common-envelope binaries, which tend to contain low-mass white dwarfs (Rebassa-Mansergas et al. 2011). As we show in Section 5, our sample may indeed have a large fraction of post-common envelope systems, which is also expected in a magnitude-limited sample since low-mass white dwarfs are more luminous for a fixed effective temperature (see Rebassa-Mansergas et al. 2011, for a discussion on how this effect affects the SDSS WDMS sample). However, it is also worth noting that Santos-García et al. (2025) gave evidence that  $\approx 30\%$  of the *Gaia* WDMS in Rebassa-Mansergas et al. (2021a) passed through a common envelope phase, a fraction that is presumable similar, or even smaller due to the larger distances considered, in the current sample. Therefore, the peak at lower white dwarf masses might also be related to the same issue with the two-body fits in VOSA mentioned above, which tends to yield lower masses than expected.

In the middle and bottom panels of Figure 6 we compare the white dwarf surface gravities and effective temperatures, respectively, of 54 objects with reliable VOSA fits that also have such values derived from available SDSS spectra (Rebassa-Mansergas et al. 2016b). It becomes obvious that not only the surface gravities, hence masses, but also the effective temperatures derived in this work seem to be systematically lower than those obtained fitting the much higher resolution SDSS spectra. This effect may be related to reddening. Even though extinction is taken into account in the VOSA fits, it could affect the white dwarfs more than their companions since they are bluer.

The secondary star effective temperatures are mainly concentrated between 2700 and 3400 K, with a peak at around 3200 K, which corresponds to M dwarfs of spectral types M3–M6 (Rebassa-Mansergas et al. 2007). This is in line with our expectations, since WDMS with earlier/later spectral type companions would tend to fall out of our regions of study.

The same pattern is observed when considering all WDMS binaries in the sample, including those objects with white dwarfs cooler than 10 000 K and less massive than 0.3  $M_{\odot}$  as indicated by their VOSA white dwarf fits. We consider this as an indicator that the secondary star fits from VOSA are more reliable than those obtained for the white dwarfs. Indeed, when comparing these temperatures with those obtained from the SDSS spectra for the 54 common objects with derived parameters<sup>6</sup>, we find that for only 12 objects ( $\approx 22\%$  of the cases) the differences are of more than 150 K. The most dramatic discrepancy is for five objects with effective temperatures higher than 3700 K as derived from their SDSS spectra, which are considered to be much cooler according to the VOSA fits. In these cases the temperature difference ranges from 500 to 1100 K.

We conclude this section by emphasising that the stellar parameters obtained from the VOSA two-body fits are generally reasonable and reliable for the secondary stars. Conversely, the white dwarf parameters should only be considered as reliable for certain ranges (effective temperatures larger than 10 000 K and masses higher than 0.3  $M_{\odot}$ ), and especially when GALEX photometry is available. That is, in those cases where the secondary

<sup>6</sup> Note that the decomposition/fitting routine of the SDSS WDMS binary spectra yields secondary spectral types rather than effective temperatures (Rebassa-Mansergas et al. 2010). We converted the spectral types into temperatures using the relation of Rebassa-Mansergas et al. (2007), which is virtually identical to the updated tables of Mamajek & Hillenbrand (2008).



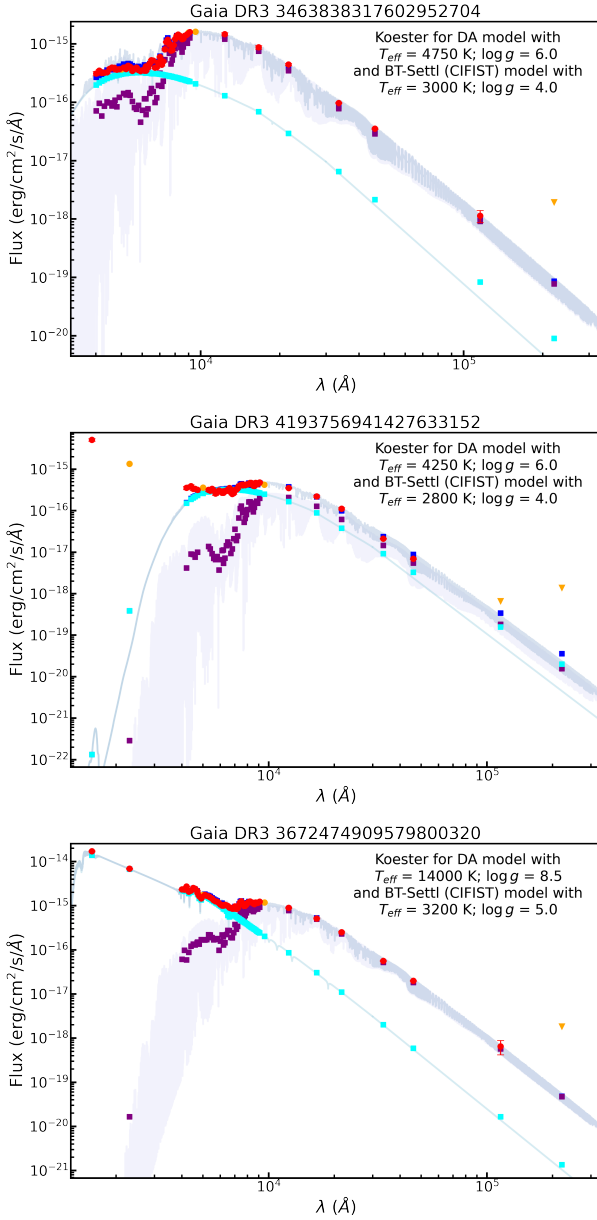


**Fig. 4.** Example of two-body VOSA fits. The top panel shows a typical MS-dominated WDMS binary in our sample. The combination of models (purple for the secondary star and cyan for the white dwarf) seem to fit relatively well the observed data (red dots). However, the effective temperature of the white dwarf is too low. Clearly, such a low-luminosity white dwarf would not be seen against a 3000 K secondary M star. The middle panel illustrates an example of a bad fit, especially in the ultraviolet range. The bottom panel shows what we consider a good fit, where the models match the observed data at all wavelengths.

star dominates the SED, too few photometric points are available in the blue, where the white dwarfs mostly contribute. As a consequence, the white dwarf parameters obtained from the fit are subject to substantial uncertainties. The stellar parameters for each target with visually acceptable two-body fits are included in Table 2.

#### 4. Comparison with other WDMS binary samples

In this section we compare our WDMS binary catalogue with other published samples from *Gaia*. For completeness, we also

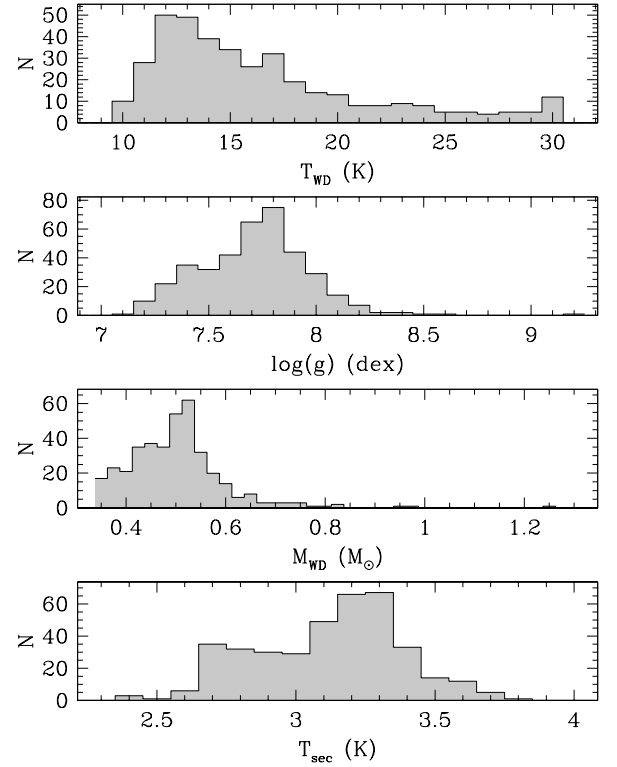


**Fig. 5.** From top to bottom, the distribution of white dwarf effective temperatures, surface gravities, masses and secondary star effective temperatures derived from 435 WDMS binaries with reliable VOSA two-body fits.

compare our catalogue to the largest spectroscopic sample of WDMS binaries previous to *Gaia*, from SDSS. We also use the results of the comparisons to estimate the completeness of our sample.

Note that we do not include a comparison with [Sidharth et al. \(2024\)](#) since their *Gaia* WDMS binaries are located in the white dwarf locus and are therefore excluded by our selection criteria. In the same way, we do not compare our catalogue with the sample of *Gaia* astrometric binaries from [Shahaf et al. \(2024\)](#) since these objects are mainly located in the main-sequence, therefore also outside of our region of study.

##### 4.1. Comparison with [Rebassa-Mansergas et al. \(2021b\)](#)

The present work aims at enlarging the volume-limited sample we provided in [Rebassa-Mansergas et al. \(2021b\)](#). Here we check whether or not the 112 WDMS candidates in that sample are included in our new catalogue. Of the 112 sources, 84 have *Gaia* DR3 spectra and 65 are common objects. Of the remaining 19 candidates, 5 and 6 are now classified in this work as single main-sequence stars and single white dwarfs, respectively, while performing the VOSA fits to their synthetic J-PAS SEDs (Section 2). We repeated the fits including GALEX, 2MASS and WISE photometry and found the same results except for two objects: *Gaia* ID 1900545847646195840 and *Gaia* ID 5490140356700680576, which display near infrared excess arguably from a low-mass companion that requires confirmation. Hence, the discrepancy between the results obtained here and those in [Rebassa-Mansergas et al. \(2021b\)](#) for these objects is due to the better-sampled optical SEDs used in this work (57

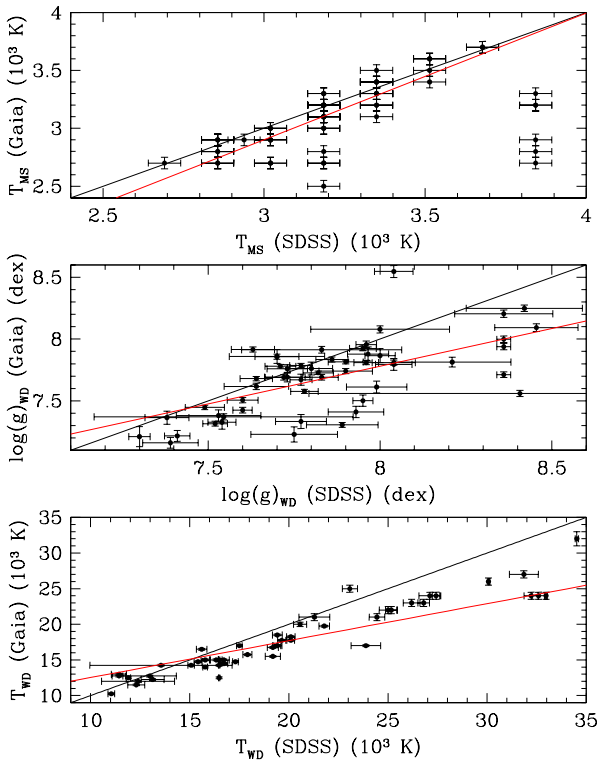


**Fig. 6.** Comparison between the white dwarf effective temperatures (bottom) and surface gravities (middle) as well as main-sequence star effective temperatures (top) for 54 WDMS binaries with VOSA reliable two-body fits and spectroscopic parameters derived from SDSS spectra. The black dashed lines indicate the one to one relation, whilst the red dashed lines are linear fits to the data (in the top panel the values above 3700 K in the horizontal axis have not been considered for being clear outliers).

points), compared to the considerably fewer optical points used in [Rebassa-Mansergas et al. \(2021b\)](#). The other 8 objects are considered as a cataclysmic variable (1), as single white dwarfs (2) or as single main-sequence stars (5) after visual inspection of their *Gaia* spectra. It is also worth noting that our new catalogue includes 31 WDMS binary candidates within 100 pc that were not included in [Rebassa-Mansergas et al. \(2021b\)](#). In all except 8 cases the visual inspection of the 31 spectra revealed one of the two components to dominate most of the flux in the optical, systems that challenge identification by any method. The top-left panel of Figure 7 provides a confusion matrix illustrating the level of agreement between the catalogues.

#### 4.2. Comparison with [Nayak et al. \(2024\)](#)

[Nayak et al. \(2024\)](#) provided a sample of 257 WDMS binaries within 100 pc by means of combining optical with ultraviolet data. This allowed to identify WDMS binaries in the MS locus of the *Gaia*  $G_{\text{abs}}$  vs.  $G_{\text{BP}} - G_{\text{RP}}$  diagram, with 28 of their sources falling in our region of study and 21 with *Gaia* spectra. Of the 21 targets, 17 are in our list, 3 are associated to a large excess and one we consider as a cataclysmic variable. The top-right panel of Figure 7 provides the corresponding confusion matrix illustrating the level of agreement between the catalogues.

#### 4.3. Comparison with [Li et al. \(2025\)](#)

[Li et al. \(2025\)](#) has provided a catalogue of  $\approx 30\,000$  WDMS binaries from *Gaia* data release 3. They used artificial intelligence neural networks to select them among the millions of available *Gaia* spectra. The advantage of their approach is that it allowed them to identify systems not only in the WDMS bridge between white dwarfs and main-sequence stars, but also outside this region. Thus, their work introduces a new methodology for identifying WDMS that can potentially reduce observational selection effects.

We compare our sample of 1312 WDMS with their list in this section. Of their 30 000 sources, 3769 are within our WDMS binary region and 962 are common objects. This means there are 2807 WDMS binary candidates in their list that we do not have and 350 candidates from our list that they do not have. Figure 7 (bottom-left) illustrates the corresponding confusion matrix between the catalogues.

We visually inspected the 2807 objects from [Li et al. \(2025\)](#) that are not in our list and identified 111 as WDMS. These objects were selected by our initial parallax and flux cuts, but were excluded because of large excess factor (82 sources) and uncertain astrometry (29 sources). The remaining 2696 objects are not considered by us as WDMS binaries according to our visual inspection, but they were flagged as such by the artificial intelligence neural network. Indeed, many of the spectra are virtually identical or closely resemble those of typical single main-sequence stars and white dwarfs and our human inspection is unable to confirm or disprove the WDMS classification. It is therefore very possible that several of those are indeed WDMS binaries. However, we also found 35 cataclysmic variables among the 2696 sources and many spectra that are difficult to interpret as representative of the WDMS binary population (see a couple of examples in Figure 8). We consider this is probably because [Li et al. \(2025\)](#) did not visually inspect the spectra of their 30 000 WDMS binary candidates to exclude objects from their list.

The 350 objects that are included in our catalogue but not in [Li et al. \(2025\)](#) all show the typical features of WDMS binaries in their spectra, with both components visible. [Li et al. \(2025\)](#) did not apply any cut in excess factor nor astrometric\_excess\_noise to their sample, only on RUWE. However, the RUWE values of the 350 sources are generally not too large ( $< \approx 1.5$ ) and we therefore do not find a clear reason why these objects were missed in their analysis.

#### 4.4. Comparison with the SDSS WDMS binary catalogue

The spectroscopic catalogue of WDMS binaries from SDSS contains 3287 objects ([Rebassa-Mansergas et al. 2016b](#)), of which 316 have *Gaia* spectra and pass our parallax/flux relative error cuts of 10% (Section 2), with 140 in our final sample. Of the 176 that we do not have, 62 were excluded due to a large excess factor, 4 because they had large RUWE values, 6 because they did not have enough points for reliable VOSA fits, 86/5 because they had  $\chi^2$  values smaller than 10 when fitting them with VOSA using white dwarf/low-mass star CIFIST models and were considered as single objects and 13 because the visual inspection of their *Gaia* spectra did not reveal clear features of both components. We also visually inspected the 86+5 objects that we considered as single objects based on their single-body VOSA fits and found the same issue, i.e. their *Gaia* spectra did not reveal clear features of both objects. This is an observational bias related to the low resolution of *Gaia*. All these objects reveal mild blue or red excess in the higher resolution SDSS spectra that are



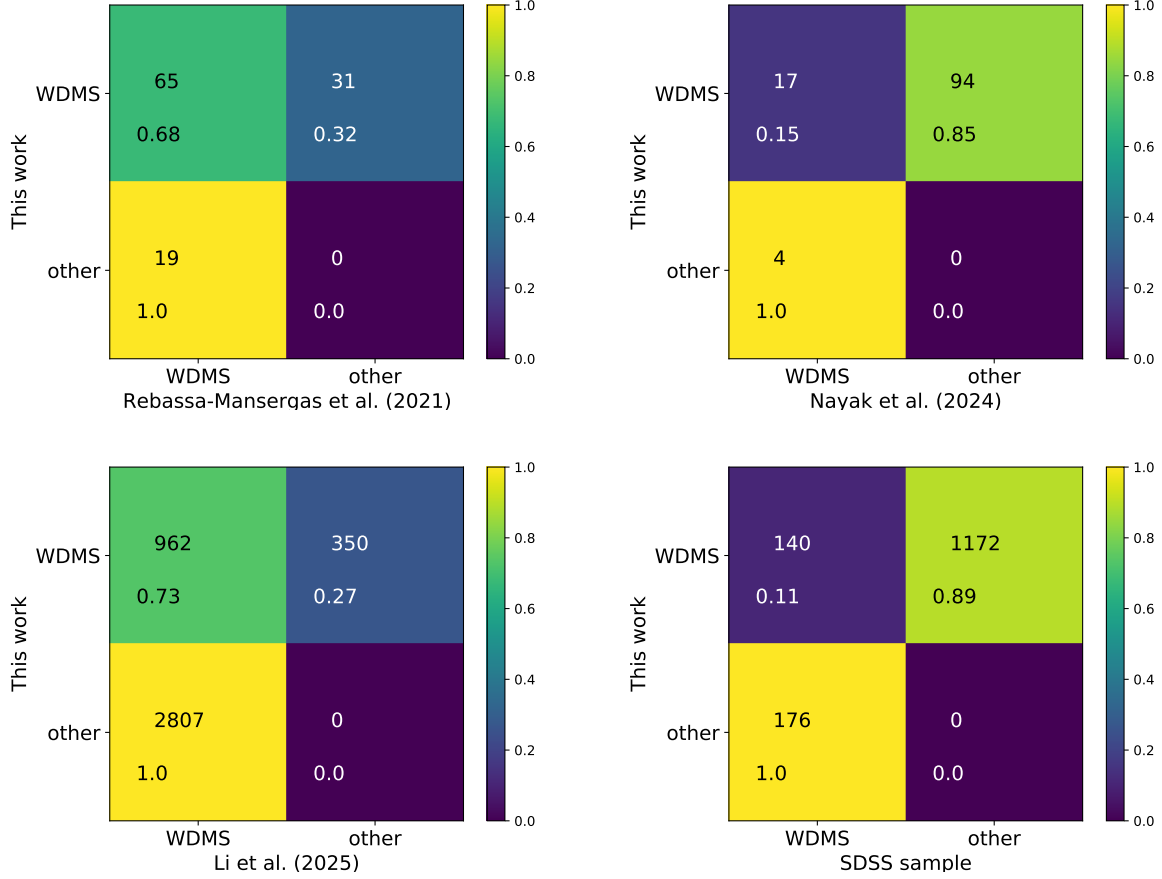


**Fig. 7.** Confusion matrices representing the level of agreement between our catalogue and other samples: [Rebassa-Mansergas et al. \(2021b\)](#) (top left), [Nayak et al. \(2024\)](#) (top right), [Li et al. \(2025\)](#) (bottom left) and the SDSS WDMS sample (bottom right). The values within the matrices indicate the number of targets falling in each category and the percentages respect to the total number of objects in each row. In particular, the top-left cells in each matrix indicate the number and fraction of common objects, whilst the diagonal cells indicate the number of objects (and fractions) missed (or not included) by the corresponding works.

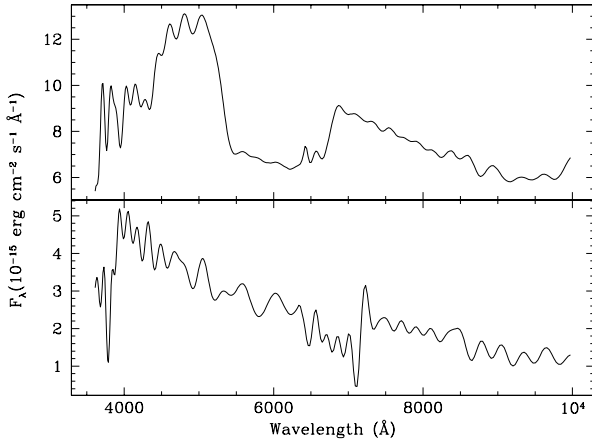


**Fig. 8.** Example spectra of WDMS binaries in the list of [Li et al. \(2025\)](#) that we do not consider as such. *Gaia* source IDs are 767397543537053312 (top) and 5952567592693723904 (bottom).

not featured in the *Gaia* spectra. Two examples are shown in Figure 9. It is worth noting that just one of the 91 WDMS that we characterise as individual sources based on their VOSA  $\chi^2$  values is included in the sample of [Li et al. \(2025\)](#), which indicates

the neural networks also struggle to find such objects, especially those with dominant white dwarf primaries.

In the bottom-right panel of Figure 7 we show the confusion matrix illustrating the level of agreement between our catalogue and the SDSS sample.

#### 4.5. Completeness of the catalogue

From the analysis in the previous sections we identify several important issues that limit the completeness of our WDMS binary catalogue, defined as  $N_{\text{cat}}/N_{\text{tot}}$ , where  $N_{\text{cat}}$  is the number of WDMS binaries in our catalogue and  $N_{\text{tot}}$  is the total number of observable WDMS within the considered region of the *Gaia*  $G_{\text{abs}}$  vs.  $G_{\text{BP}} - G_{\text{RP}}$  diagram. Ideally,  $N_{\text{cat}}/N_{\text{tot}}$  should be close to 1.

To begin with, not all the WDMS binaries with *Gaia* photometry and astrometry have spectra. For example, of the 3287 SDSS WDMS binaries, 3089 have *Gaia* photometry and astrometry, but only 316 have *Gaia* spectra (Section 4.4). In the 100 pc samples of [Nayak et al. \(2024\)](#) and [Rebassa-Mansergas et al. \(2021b\)](#), 21 out of 28 and 84 out of 112, respectively, have *Gaia* spectra (Sections 4.2 and 4.1). Thus, at 100 pc the fraction of WDMS with *Gaia* spectra seems to be  $\approx 75\%$ , and drops significantly to  $\approx 10\%$  for distances as large as 1.5 kpc (which is ap-

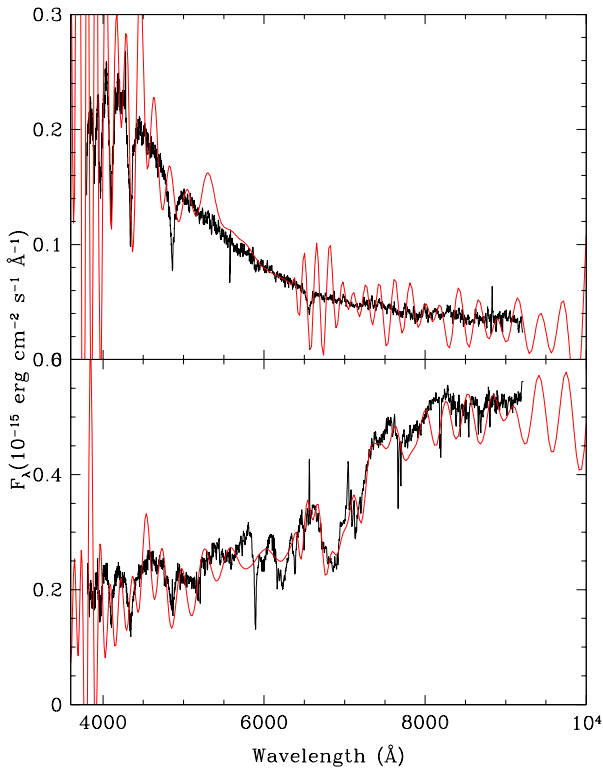


**Fig. 9.** Example spectra of WDMS binaries displaying red (top; *Gaia* ID 904263926328520320) and blue (bottom; *Gaia* ID 686844023151243904) excess clearly visible in the SDSS spectra (black) but diluted in the *Gaia* spectra (red).

proximately the maximum distance at which the SDSS WDMS binaries are located; [Rebassa-Mansergas et al. 2010](#)).

In addition, in Section 4.3 we identified 111 WDMS binaries from [Li et al. \(2025\)](#) that are not in our catalogue because of the excess factor and astrometry cuts applied in Section 2. In the same way, 66 SDSS WDMS binaries with *Gaia* spectra are not in our final list because of the same reasons (Section 4.4). Since our sample consists of 1312 sources and 177 targets are confirmed WDMS that did not make it to our catalogue, this means that we missed at least  $\approx 12\%$  of the WDMS binaries. A further complication is the fact that it becomes increasingly more difficult to identify WDMS binaries with mild blue/red excess in their optical spectra due to the low resolution of *Gaia*. As mentioned in Section 4.4, 91 SDSS WDMS binaries of such characteristics were excluded from our sample since we considered them as individual sources based on the results from the VOSA fits. Knowing that our final sample is  $N_{\text{cat}} = 1312$  and recalling that  $N_{\text{tot}}$  is the total number of observable WDMS within the considered region, then:

$$N_{\text{tot}} \times f_{\text{spec}} \times f_{\text{cuts}} \times f_{\text{vis}} = N_{\text{cat}}, \quad (4)$$

where  $f_{\text{spec}}$  is the fraction of expected WDMS with *Gaia* spectra ( $\approx 0.1$ ; this is a lower limit since the fraction depends on the distance considered),  $f_{\text{cuts}}$  is the fraction of expected WDMS with *Gaia* spectra that we recovered after applying our cuts in astrometry and excess factor ( $\approx 0.88$ ; this is an upper limit since at least a fraction of 0.12 are expected to be missed, as discussed above) and  $f_{\text{vis}}$  is the fraction of WDMS with *Gaia* spectra satisfying our quality cuts that we expect to display both components (or at least significant blue/red excess) in their spectra ( $\approx 0.6$ ;

since 40% of the SDSS WDMS satisfying our quality cuts do not show both components in their low-resolution *Gaia* spectra and are even considered as single objects when performing the VOSA fits (Section 4.4)).

From the above fractions and Equation 4, we derive a value of  $N_{\text{tot}} = 24\,848$ , that is a lower limit for the completeness  $N_{\text{cat}}/N_{\text{tot}}$  of  $\approx 5\%$  for our catalogue, or  $\approx 50\%$  if we consider WDMS with available *Gaia* spectra. This is not surprising given the large number of observational biases involved. On the positive side, the presented catalogue, which represents the tip of the iceberg of the underlying WDMS population, is statistically large enough and is well-characterised. That is, we have obtained reliable estimates of the percentages of WDMS systems missed due to each observational bias, all of which can be incorporated into numerical simulations. This allows synthetic populations to be meaningfully compared with the observed one, providing tighter constraints on binary star formation and evolution (see, for example, [Santos-García et al. 2025](#), who performed this exercise with the 112 *Gaia* WDMS binaries within 100 pc of [Rebassa-Mansergas et al. 2021b](#)).

## 5. Eclipsing systems

Given that a significant number of the systems in our sample are likely to have evolved through a common-envelope phase, and consequently have short orbital periods, we should expect a fraction to have an orbital inclination such that they are seen to eclipse. We cross-matched the 1312 WDMS binaries in the sample with the catalogue of eclipsing WDMS binaries from the Zwicky Transient Facility (ZTF; [Dekany et al. 2020](#)) by van Roestel et al. in prep.) returning 63 matches. 20 of these are in the sub-sample of 435 systems with good VOSA two-body fits and therefore have estimates of their parameters. Follow-up observations of these objects will hence allow determining masses and radii that can be directly compared to those estimated here. In order to identify any southern eclipsing systems we also checked photometry from the Catalina Real-time Transient Survey DR3 (CRTS; [Drake et al. 2009](#)), following the method outlined in [Parsons et al. \(2013\)](#) and only targeted objects outside of the ZTF footprint. We found four eclipsing systems, although we note that CRTS does not go as deep as ZTF. We obtained the orbital periods of the eclipsing systems we have identified in both surveys via applying standard Lomb-Scargle periodograms to the light-curves, and then using a box least squares periodogram to refine the periods (see some examples in Figure 10). The results are provided in Table 2.

Estimates for the fraction of eclipsing post-common-envelope binaries, PCEBs, containing a white dwarf and a low-mass main-sequence companion typically lie around 12-18% ([Parsons et al. 2013](#); [Santos-García et al. 2025](#)), but the exact fraction depends on the orbital period distribution as well as the mass, and therefore radius, distributions of the two stars. The number of eclipsing systems within the sample can therefore provide a lower limit on the fraction of PCEBs in our catalogue (a lower limit because not all eclipsing systems will be detected). Of the 1312 systems in the full sample, 920 of these are accessible to the ZTF survey (declination  $> -31$  degrees), of which 63 are found to be eclipsing. Assuming that eclipsing systems account for 12-18% of PCEBs, this suggests that at least  $\approx 38 - 57\%$  of the full sample are PCEBs. Performing the same analysis for the sub-sample of 435 systems with reliable fits to the *Gaia* spectroscopy (Section 3 and Figure 5) we find that at least  $\approx 31 - 46\%$  of these are PCEBs.

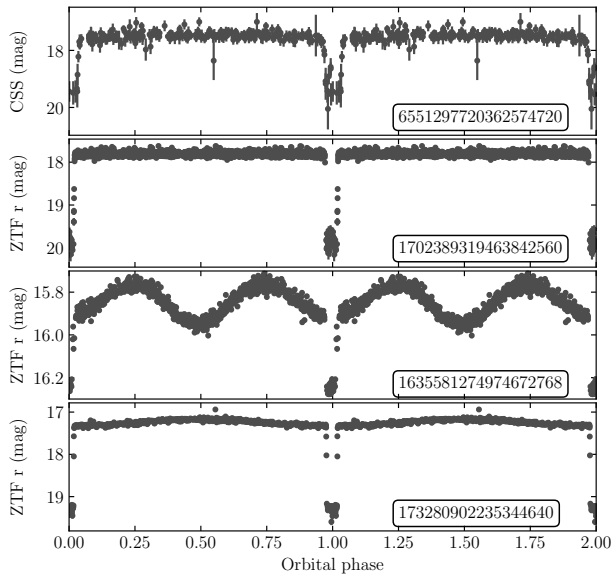


**Fig. 10.** CRTS and ZTF phase-folded photometry for 4 of the 67 eclipsing systems in the sample. Two orbits are shown for clarity and the respective *Gaia* DR3 source IDs are displayed in the bottom right of each panel.

The estimated PCEB fraction among WDMS in our sample seems to be higher than expected. Numerical simulations indicate that PCEBs account for approximately 25-30% of the total WDMS population (Willems & Kolb 2004; Toonen & Nelemans 2013), including the *Gaia* 100 pc sample (Santos-García et al. 2025). Observational studies reveal similar PCEB fractions (Schreiber et al. 2010; Nebot Gómez-Morán et al. 2011; Rebassa-Mansergas et al. 2011). It is therefore plausible that some observational biases affect the *Gaia* WDMS sample, which favour the detection of eclipsing systems. For example, as mentioned in Section 3, a magnitude-limited WDMS sample favours the detection of low-mass white dwarfs, since these are more luminous for a fixed effective temperature (Rebassa-Mansergas et al. 2011). Moreover, the wider the orbital separations, the more likely it is for *Gaia* to resolve the two components, which would imply a bias towards shorter period systems. In the same way, wide binaries are more likely to be associated to larger values of RUWE and/or excess factor, objects that may be excluded by our quality cuts. It is also worth noting that our estimated PCEB fractions assume that the cuts performed in magnitude-colour space do not impact the likelihood of a PCEBs to eclipse. For a more accurate estimate of the PCEB fraction, population synthesis techniques (e.g. Santos-García et al. 2025) will be required.

## 6. Summary and conclusions

During the last two decades it has been shown that WDMS binaries are of great use to improve our understanding of a wide range of topics in astronomy. This relies on the existence of statistically large and well-defined samples that allow characterising the biases affecting the observed populations. In this sense, in this work we have built a sample of 1312 WDMS binaries via mining the spectroscopic content of the data release 3 of *Gaia*.

The catalogue is expected to be  $\approx 50$  per cent complete. The missing targets are predominantly expected to be objects with large values of RUWE and/or the excess noise parameters, as well as objects with mild blue or red excess in their optical spec-

tra, features that are diluted in the low-resolution *Gaia* spectra. The identification of such WDMS is expected to improve by using artificial intelligence algorithms applied to the *Gaia* spectra (Echeverry et al. 2022; Li et al. 2025; Pérez-Couto et al. 2025), although they fail to detect a non-negligible fraction of WDMS binaries and often misclassify irregular spectra. Moreover, the completeness dramatically drops to  $\approx 5$  per cent (lower limit) if we consider that not all WDMS binaries in *Gaia* have available spectra. However, despite these issues, our catalogue is very well characterised in terms of implemented photometric and astrometric cuts and observational biases and hence can be directly compared to synthetic samples that reproduce the WDMS binary population in the Galaxy to constrain, for example, binary star evolution (Santos-García et al. 2025). In addition, the study of exotic objects in the sample, such as the 67 identified eclipsing systems (which represent 5% of the total sample), allows to place tighter constraints on the mass-radius relation of both white dwarfs and low-mass main-sequence stars (Parsons et al. 2017, 2018).

We find the catalogue to be dominated by binaries in which the main-sequence companion contributes more in the optical spectral energy distribution. Because of this, the stellar parameters that we derived for most of the white dwarfs in these objects should be considered with caution. Future follow-up spectroscopic observations at higher resolution are therefore desired for better characterization of the white dwarfs. Hence, these sources are excellent supplementary targets for the forthcoming White Dwarf Binary Survey (Toloza et al. 2023) implemented in the overall 4MOST survey (4-metre Multi-Object Spectroscopic Telescope; de Jong et al. 2022).

## 7. Data availability

Table 2 is only available in electronic form at the CDS via anonymous ftp to cdsarc.u-strasbg.fr (130.79.128.5) or via <http://cdsweb.u-strasbg.fr/cgi-bin/qcat?J/A+A/>.

**Acknowledgements.** We thank Enrique García-Zamora for helping with the construction of the confusion matrices. We thank the anonymous referee for the comments and suggestions on the manuscript. This work was partially supported by the Spanish MINECO grant PID2023-148661NB-I00 and by the AGAUR/Generalitat de Catalunya grant SGR-386/2021. This work was partially supported by the Spanish Virtual Observatory (<https://svo.cab.inta-csic.es/projectfundedbyMCIN/AEI/10.13039/501100011033/>) through grant PID2023-146210NB-I00. RMO is funded by INTA through grant PRE-OBSERVATORIO. RR acknowledges support from Grant RYC2021-030837-I, funded by MCIN/AEI/ 10.13039/501100011033 and by “European Union NextGeneration EU/PRTR”. MC acknowledges grant RYC2021-032721-I, funded by MCIN/AEI/10.13039/501100011033 and by the European Union NextGeneration EU/PRTR. This work presents results from the European Space Agency (ESA) space mission *Gaia*. *Gaia* data are being processed by the *Gaia* Data Processing and Analysis Consortium (DPAC). Funding for the DPAC is provided by national institutions, in particular the institutions participating in the *Gaia* MultiLateral Agreement (MLA). The *Gaia* mission website is <https://www.cosmos.esa.int/gaia>. The *Gaia* archive website is <https://archives.esac.esa.int/gaia>. This job has made use of the Python package GaiaXPY, developed and maintained by members of the *Gaia* Data Processing and Analysis Consortium (DPAC), and in particular, Coordination Unit 5 (CU5), and the Data Processing Centre located at the Institute of Astronomy, Cambridge, UK (DPCI).

## References

- Allard, F., Homeier, D., Freytag, B., Schaffenberger, W., & Rajpurohit, A. S. 2013, *Memorie della Società Astronomica Italiana Supplementi*, 24, 128
- Althaus, L. G., Miller Bertolami, M. M., & Corsico, A. H. 2013, *A&A*, 557, A19
- Anguiano, B., Majewski, S. R., Stassun, K. G., et al. 2022, *AJ*, 164, 126
- Arseneau, S., Chandra, V., Hwang, H.-C., et al. 2024, *ApJ*, 963, 17
- Bailer-Jones, C. A. L. 2023, *AJ*, 166, 269



- Barrientos, M. & Chanamé, J. 2021, *ApJ*, 923, 181
- Bayo, A., Rodrigo, C., Barrado Y Navascués, D., et al. 2008, *A&A*, 492, 277
- Belokurov, V., Penoyre, Z., Oh, S., et al. 2020, *MNRAS*, 496, 1922
- Benitez, N., Dupke, R., Moles, M., et al. 2014, arXiv e-prints, arXiv:1403.5237
- Bianchi, L., Shiao, B., & Thilker, D. 2017, *ApJS*, 230, 24
- Brown, A. J., Parsons, S. G., van Roestel, J., et al. 2023, *MNRAS*, 521, 1880
- Bruch, A. & Diaz, M. P. 1998, *AJ*, 116, 908
- Camacho, J., Torres, S., García-Berro, E., et al. 2014, *A&A*, 566, A86
- Camisassa, M. E., Althaus, L. G., Córscico, A. H., et al. 2019, *A&A*, 625, A87
- Camisassa, M. E., Althaus, L. G., Córscico, A. H., et al. 2016, *ApJ*, 823, 158
- Chen, X., Wang, S., Deng, L., et al. 2020, *ApJS*, 249, 18
- Chiti, F., van Saders, J. L., Heintz, T. M., et al. 2024, *ApJ*, 977, 15
- Cojocaru, R., Rebassa-Mansergas, A., Torres, S., & García-Berro, E. 2017, *MNRAS*, 470, 1442
- Cui, X.-Q., Zhao, Y.-H., Chu, Y.-Q., et al. 2012, *Research in Astronomy and Astrophysics*, 12, 1197
- Davis, P. J., Kolb, U., & Willems, B. 2010, *MNRAS*, 403, 179
- de Jong, R. S., Bellido-Tirado, O., Brynnel, J. G., et al. 2022, in *Society of Photo-Optical Instrumentation Engineers (SPIE) Conference Series*, Vol. 12184, *Ground-based and Airborne Instrumentation for Astronomy IX*, ed. C. J. Evans, J. J. Bryant, & K. Motohara, 1218414
- Dekany, R., Smith, R. M., Riddle, R., et al. 2020, *PASP*, 132, 038001
- Drake, A. J., Djorgovski, S. G., Mahabal, A., et al. 2009, *ApJ*, 696, 870
- Echeverry, D., Torres, S., Rebassa-Mansergas, A., & Ferrer-Burjachs, A. 2022, *A&A*, 667, A144
- Eisenstein, D. J., Weinberg, D. H., Agol, E., et al. 2011, *AJ*, 142, 72
- Evans, D. W., Riello, M., De Angeli, F., et al. 2018, *A&A*, 616, A4
- Farihi, J., Hoard, D. W., & Wachter, S. 2010, *ApJS*, 190, 275
- Gaia Collaboration, Brown, A. G. A., Vallenari, A., et al. 2018, *A&A*, 616, A1
- Gaia Collaboration, Montegriffo, P., Bellazzini, M., et al. 2023, *A&A*, 674, A33
- Garbutt, J. A., Parsons, S. G., Toloza, O., et al. 2024, *MNRAS*, 529, 4840
- Gentile Fusillo, N. P., Tremblay, P.-E., Gänsicke, B. T., et al. 2019, *MNRAS*, 482, 4570
- Grondin, S. M., Drout, M. R., Nordhaus, J., et al. 2024, *ApJ*, 976, 102
- Hallakoun, N., Shahaf, S., Mazeh, T., Toonen, S., & Ben-Ami, S. 2024, *ApJ*, 970, L11
- Koester, D. 2010, *Mem. Soc. Astron. Italiana*, 81, 921
- Kosakowski, A., Kilic, M., Brown, W. R., Bergeron, P., & Kupfer, T. 2022, *MNRAS*, 516, 720
- Lallement, R., Vergely, J. L., Valette, B., et al. 2014, *A&A*, 561, A91
- Li, J., Ting, Y.-S., Rix, H.-W., et al. 2025, arXiv e-prints, arXiv:2501.14494
- Lindgren, L., Lammers, U., Hobbs, D., et al. 2012, *A&A*, 538, A78
- Mamajek, E. E. & Hillenbrand, L. A. 2008, *ApJ*, 687, 1264
- Marín-Franch, A., Chueca, S., Moles, M., et al. 2012, in *Society of Photo-Optical Instrumentation Engineers (SPIE) Conference Series*, Vol. 8450, *Modern Technologies in Space- and Ground-based Telescopes and Instrumentation II*, ed. R. Navarro, C. R. Cunningham, & E. Prieto, 84503S
- Marsh, T. R., Gänsicke, B. T., Hümmerich, S., et al. 2016, *Nature*, 537, 374
- Mowlavi, N., Holl, B., Lecoœur-Taïbi, I., et al. 2023, *A&A*, 674, A16
- Nayak, P. K., Ganguly, A., & Chatterjee, S. 2024, *MNRAS*, 527, 6100
- Nebot Gómez-Morán, A., Gänsicke, B. T., Schreiber, M. R., et al. 2011, *A&A*, 536, A43
- Nebot Gómez-Morán, A., Schwöpe, A. D., Schreiber, M. R., et al. 2009, *A&A*, 495, 561
- O'Donoghue, D., Koen, C., Kilkeny, D., et al. 2003, *MNRAS*, 345, 506
- Paczynski, B. 1976, in *IAU Symposium*, Vol. 73, *Structure and Evolution of Close Binary Systems*, ed. P. Eggleton, S. Mitton, & J. Whelan, 75
- Parsons, S. G., Agurto-Gangas, C., Gänsicke, B. T., et al. 2015, *MNRAS*, 449, 2194
- Parsons, S. G., Brown, A. J., Casewell, S. L., et al. 2025, *MNRAS*, 537, 2112
- Parsons, S. G., Gänsicke, B. T., Marsh, T. R., et al. 2017, *MNRAS*, 470, 4473
- Parsons, S. G., Gänsicke, B. T., Marsh, T. R., et al. 2018, *MNRAS*, 481, 1083
- Parsons, S. G., Gänsicke, B. T., Marsh, T. R., et al. 2013, *MNRAS*, 429, 256
- Parsons, S. G., Rebassa-Mansergas, A., Schreiber, M. R., et al. 2016, *MNRAS*, 463, 2125
- Penoyre, Z., Belokurov, V., & Evans, N. W. 2022, *MNRAS*, 513, 5270
- Pérez-Couto, X., Manteiga, M., & Villaver, E. 2025, arXiv e-prints, arXiv:2503.04672
- Priyatikanto, R., Knigge, C., Scaringi, S., Brink, J., & Buckley, D. A. H. 2022, *MNRAS*, 516, 1183
- Pyrzas, S., Gänsicke, B. T., Brady, S., et al. 2012, *MNRAS*, 419, 817
- Pyrzas, S., Gänsicke, B. T., Marsh, T. R., et al. 2009, *MNRAS*, 394, 978
- Raddi, R., Rebassa-Mansergas, A., Torres, S., et al. 2025, *A&A*, 695, A131
- Raddi, R., Torres, S., Rebassa-Mansergas, A., et al. 2022, *A&A*, 658, A22
- Rebassa-Mansergas, A., Anguiano, B., García-Berro, E., et al. 2016a, *MNRAS*, 463, 1137
- Rebassa-Mansergas, A., Gänsicke, B. T., Rodríguez-Gil, P., Schreiber, M. R., & Koester, D. 2007, *MNRAS*, 382, 1377
- Rebassa-Mansergas, A., Gänsicke, B. T., Schreiber, M. R., Koester, D., & Rodríguez-Gil, P. 2010, *MNRAS*, 402, 620
- Rebassa-Mansergas, A., Gänsicke, B. T., Schreiber, M. R., et al. 2008, *MNRAS*, 390, 1635
- Rebassa-Mansergas, A., Maldonado, J., Raddi, R., et al. 2021a, *MNRAS*, 505, 3165
- Rebassa-Mansergas, A., Maldonado, J., Raddi, R., et al. 2023, *MNRAS*, 526, 4787
- Rebassa-Mansergas, A., Nebot Gómez-Morán, A., Schreiber, M. R., et al. 2012, *MNRAS*, 419, 806
- Rebassa-Mansergas, A., Nebot Gómez-Morán, A., Schreiber, M. R., Girven, J., & Gänsicke, B. T. 2011, *MNRAS*, 413, 1121
- Rebassa-Mansergas, A., Parsons, S. G., Dhillon, V. S., et al. 2019, *Nature Astronomy*, 3, 553
- Rebassa-Mansergas, A., Parsons, S. G., García-Berro, E., et al. 2017, *MNRAS*, 466, 1575
- Rebassa-Mansergas, A., Ren, J. J., Parsons, S. G., et al. 2016b, *MNRAS*, 458, 3808
- Rebassa-Mansergas, A., Schreiber, M. R., & Gänsicke, B. T. 2013, *MNRAS*, 429, 3570
- Rebassa-Mansergas, A., Solano, E., Jiménez-Esteban, F. M., et al. 2021b, *MNRAS*, 506, 5201
- Ren, J. J., Raddi, R., Rebassa-Mansergas, A., et al. 2020, *ApJ*, 905, 38
- Ren, J. J., Rebassa-Mansergas, A., Parsons, S. G., et al. 2018, *MNRAS*, 477, 4641
- Riello, M., De Angeli, F., Evans, D. W., et al. 2021, *A&A*, 649, A3
- Rybizki, J., Green, G. M., Rix, H.-W., et al. 2022, *MNRAS*, 510, 2597
- Santos-García, A., Torres, S., Rebassa-Mansergas, A., & Brown, A. J. 2025, *A&A*, 695, A161
- Schreiber, M. R., Belloni, D., Gänsicke, B. T., Parsons, S. G., & Zorotovic, M. 2021, *Nature Astronomy*, 5, 648
- Schreiber, M. R., Gänsicke, B. T., Rebassa-Mansergas, A., et al. 2010, *A&A*, 513, L7
- Shahaf, S., Hallakoun, N., Mazeh, T., et al. 2024, *MNRAS*, 529, 3729
- Sidharth, A. V., Shridharan, B., Mathew, B., et al. 2024, *A&A*, 690, A68
- Skrutskie, M. F., Cutri, R. M., Stiening, R., et al. 2006, *AJ*, 131, 1163
- Toloza, O., Rebassa-Mansergas, A., Raddi, R., et al. 2023, *The Messenger*, 190, 4
- Toonen, S. & Nelemans, G. 2013, *A&A*, 557, A87
- Torres, S., Canals, P., Jiménez-Esteban, F. M., Rebassa-Mansergas, A., & Solano, E. 2022, *MNRAS*, 511, 5462
- Webbink, R. F. 2008, in *Astrophysics and Space Science Library*, Vol. 352, *Astrophysics and Space Science Library*, ed. E. F. Milone, D. A. Leahy, & D. W. Hobill, 233
- Willems, B. & Kolb, U. 2004, *A&A*, 419, 1057
- Wright, N. J., Newton, E. R., Williams, P. K. G., Drake, J. J., & Yadav, R. K. 2018, *MNRAS*, 479, 2351
- Yamaguchi, N., El-Badry, K., Rees, N. R., et al. 2024, *PASP*, 136, 084202
- Zhao, J. K., Oswalt, T. D., Willson, L. A., Wang, Q., & Zhao, G. 2012, *ApJ*, 746, 144
- Zorotovic, M., Schreiber, M. R., Gänsicke, B. T., & Nebot Gómez-Morán, A. 2010, *A&A*, 520, A86
- Zorotovic, M., Schreiber, M. R., Parsons, S. G., et al. 2016, *MNRAS*, 457, 3867